

Journal of Materials Chemistry A

Accepted Manuscript



This is an *Accepted Manuscript*, which has been through the Royal Society of Chemistry peer review process and has been accepted for publication.

Accepted Manuscripts are published online shortly after acceptance, before technical editing, formatting and proof reading. Using this free service, authors can make their results available to the community, in citable form, before we publish the edited article. We will replace this *Accepted Manuscript* with the edited and formatted *Advance Article* as soon as it is available.

You can find more information about *Accepted Manuscripts* in the [Information for Authors](#).

Please note that technical editing may introduce minor changes to the text and/or graphics, which may alter content. The journal's standard [Terms & Conditions](#) and the [Ethical guidelines](#) still apply. In no event shall the Royal Society of Chemistry be held responsible for any errors or omissions in this *Accepted Manuscript* or any consequences arising from the use of any information it contains.

Key components to the recent performance increases of solution processed non-fullerene small molecule acceptors

Seth M. McAfee,¹ Jessica M. Toppo,² Ian G. Hill,^{2*} and Gregory C. Welch^{1*}

*Department of Chemistry¹, Department of Physics²
Dalhousie University, 6274 Coburg Road
Halifax, Nova Scotia, Canada B3H 4R2*

ian.hill@dal.ca, gregory.welch@dal.ca

Key Words: Organic Semiconductors, Organic Solar Cells, Small Molecules, Electron Acceptors, Non-fullerene, Solution Processed

Abstract

In recent years, the intensive development of π -conjugated small molecule acceptors has yielded viable alternatives to fullerene acceptors in state-of-the-art organic photovoltaic devices. Small molecule acceptors are designed to replicate the favourable electronic properties of fullerenes and to overcome their inherent optical and stability deficiencies. Concurrently, advances in device engineering through rigorous optimization have seen the development of intricate device architectures and led to impressive performance increases. This review highlights a number of recent high performance non-fullerene acceptors, focusing on the design of π -conjugated structures, device optimization and the ensuing power conversion efficiencies.

1. Introduction

Solution processed organic photovoltaic devices (OPVs) have emerged as a promising clean energy generating technology due to their potential for low-cost manufacturing *via* printing or coating techniques.¹⁻⁷ Traditionally, the field of OPVs has been dominated by the conjugated polymer-fullerene bulk heterojunction (BHJ) solar cell;⁸⁻¹⁰ however, the use of soluble organic small molecules in place of both polymer and fullerene components in BHJ solar cells represents a promising alternative. The key advantages of molecular alternatives to fullerene acceptors are well-known,¹¹⁻¹³ and this has led to a rise in the development of non-fullerene electron accepting small molecules. The deficiencies of fullerene acceptors are related to their cost, synthetic accessibility, poor light harvesting properties and photochemical stability in air. Further details pertaining to the history of fullerene acceptors and their small molecule alternatives have been reviewed in our previous work,¹⁴ and several other publications.¹⁵⁻²⁰

Non-fullerene small molecule acceptors can be designed from low-cost building blocks, assembled through straightforward synthetic protocols, and easily purified, rather than the expensive and demanding synthesis of fullerene acceptors. In terms of material properties, small molecule acceptors have large extinction coefficients, providing

acceptor domains with complementary light harvesting (to their respective donor components) in contrast to weakly absorbing fullerene acceptors. Considering the remarkable progress in the development of small molecule non-fullerene acceptors within the last year, a timely review of high performance non-fullerene acceptors is needed to keep up with their rapidly evolving development and guide researchers towards further improvements.

In the pursuit of new electron accepting materials, the deficiencies of fullerene acceptors are well known, but the reasons for which they remain excellent electron acceptors cannot be understated. Li *et al.* have recently summarized these characteristics.²¹ The electrochemical properties of fullerenes are highlighted by the existence of several low-lying excited states,²² providing a density of LUMO levels at similar energies, facilitating efficient charge separation without compromising charge recombination.^{23,24} Structurally, the large π -conjugated structure can efficiently delocalize electrons, and the rigidity facilitates aggregation into phase-separated morphologies ideal for charge separation and transport.^{25–28} The spherical three-dimensional structure is also an important feature, and can decrease the Coulombic barrier for charge separation while also inducing entropic effects to enable isotropic charge transport.^{29–32} It has been demonstrated that the tunability of small molecule acceptors can target the favourable properties of fullerene acceptors, and coupled with their aforementioned benefits, reach improved efficiencies.

Reviewed hereinafter are a collection of high performance non-fullerene acceptors that, when paired with appropriate donor materials, have led to the fabrication of solar cell devices with power conversion efficiencies (PCE) exceeding 3.0 % within the past year. Considering the favourable properties of fullerenes, the designs of these materials are generally focused on one or more of the following strategies: (1) electron deficient building blocks and extended π -conjugated frameworks to promote charge delocalization (2) dimeric or higher oligomeric structures to access a large density of states at the LUMO and (3) steric demand along the molecular backbone to enforce a non-planar geometry and target a blend morphology that is efficient for charge separation and transport.

In this review of recent high performance non-fullerene acceptors we hope to provide the reader with guidelines for the development of new fullerene alternatives based on current successful strategies. Foremost, it is evident that materials design is not the principal consideration for the development of non-fullerene acceptors, where donor selection, device engineering and active layer processing are equally important components to realizing high PCEs. In contrast to the development of donor materials, where common practice involves screening new materials with fullerene acceptors in standard device architecture to determine the best material for further optimization, there does not exist a standard procedure for evaluating non-fullerene acceptors. Therefore, we have organized this review to highlight the importance of appropriate donor selection, device engineering, and active layer processing conditions before engaging in the discussion pertaining to the design of new small molecule acceptors.

2. Device Engineering

Accompanying the development of new materials, advances in device engineering have proven to be crucial to achieve high efficiencies. Beyond the choice of conventional or inverted device architecture, there are many intricate components to consider, including the interfacial layers, active layer blend thickness, ratios and processing, which includes solvent additives and post-deposition annealing techniques. These components of device engineering are summarized in the following section to emphasize the importance for rigorous device optimization to reach high efficiencies.

2.1 Architecture

High performance non-fullerene acceptor BHJ devices are generally built in one of two anode/BHJ/cathode architectures: the “conventional” architecture, in which the transparent conductive electrode coated substrate (generally indium tin oxide, ITO coated glass substrate) acts as the anode, collecting holes; and the “inverted” architecture, in which the transparent conductive electrode acts as the cathode, collecting electrons (Figure 2.1). The inverted device architecture gained widespread attention relatively recently upon publication of the record breaking polymer-fullerene inverted device by He *et al.*, one of the first examples of a system in which the BHJ inverted device outperformed the conventional device. The superior performance of the inverted device was attributed to improved optical absorption and the creation of an efficient charge-carrier collecting ohmic contact at the ITO cathode, produced by including poly[(9,9-bis(3'-(*N,N*-dimethylamino)propyl)-2,7-fluorene)-alt-2,7-(9,9-dioctylfluorene)] (PFN) as an interlayer.³³

High PCEs have been achieved by non-fullerene acceptor blend devices in both architectures, but several recent publications report that changing from the conventional to inverted structure can improve PCE. For example, Zhong *et al.* demonstrated that a 3:7 mass ratio blend of polythieno[3,4-*b*]-thiophene-co-benzodithiophene (**PTB7**) polymer donor with a helical perylene diimide (**Helical PDI**) acceptor achieved PCEs of 3.5 % in a conventional device architecture and 4.5 % in an inverted structure.³⁴ Similarly, Zang *et al.* found that BHJ blends of **PTB7-Th** donor with bay-linked perylene bisimide (**di-PDI**) achieved a higher PCE of 5.3 % in an inverted device architecture than of 4.2 % in the conventional structure.³⁵ Conventional device PCE of 4.2 % and inverted device PCE of 5.0 % were reported by Li *et al.* for blends of a thiazolothiazolodithienosilole copolymer donor (**PSEHTT**) with non-fullerene acceptor 2,5-bis(8-(17-phenyl)-7,9,16,18-tetraazabenzodifluoranthene-3,4,12,13-tetracarboxylic acid diimide)thiophene (**DBFI-T**).²¹ Lu *et al.* found that optimized blends of polymer donor **PBDTTT-CT** with a perylene diimide dimer acceptor **Bis-PDI-T-MO** achieved 3.3 % PCE in the conventional architecture and 4.2 % in the inverted architecture, though notably, with different optimal processing amounts of the solvent additive 1,8-diiodooctane (DIO), related to tailoring the surface blend composition.³⁶

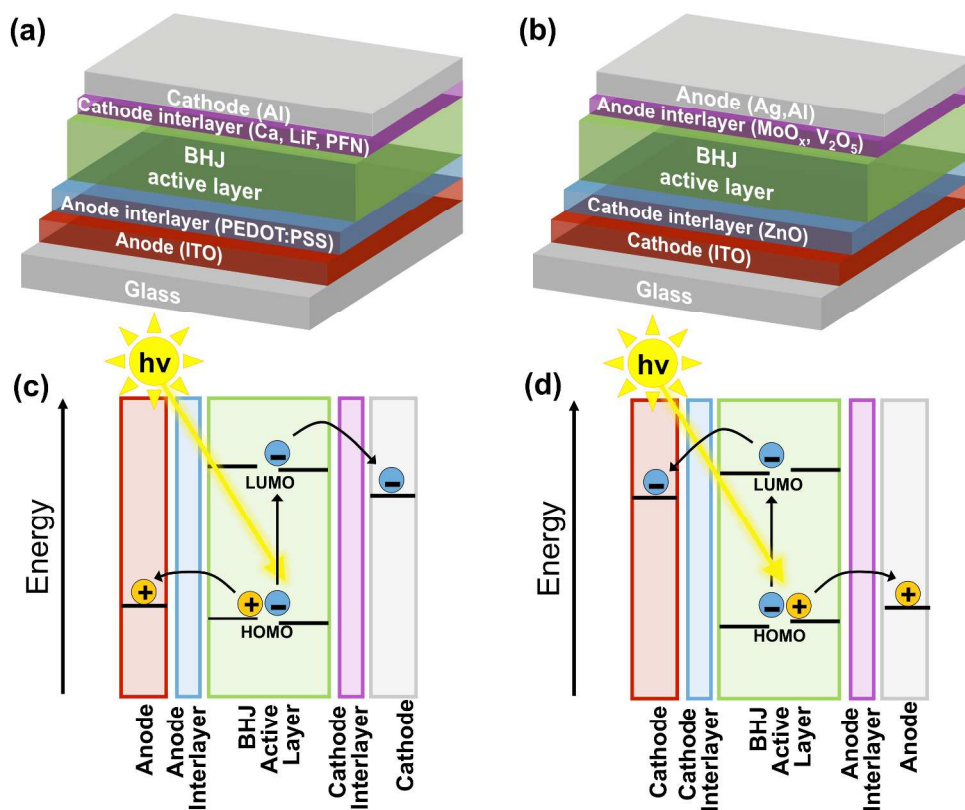


Figure 2.1. BHJ device schematics (a) conventional architecture, (b) inverted architecture, and energy level diagrams for (c) conventional and (d) inverted devices.

2.2 Interfacial Layers

Interfacial layers (or interlayers) are essentially used to tailor energy levels and electric fields within both conventional and inverted devices in order to facilitate efficient charge carrier collection from BHJ active materials by electrodes.³⁷ They can also influence the film morphology of adjacent layers. Herein, we summarize the interlayers used in recent high performance non-fullerene solar cell devices with PCEs greater than 3.0 % (structures shown in Supporting Information).

In conventional non-fullerene acceptor device architectures, the work function of the cathode (typically Al) is most commonly reduced by the inclusion of a thin evaporated layer of Ca³⁸⁻⁴² (~5-15 nm thick) or LiF^{21,43} (~1 nm thick). Both Ca and LiF interlayers may be susceptible to oxidation (LiF may dissociate to produce reactive and diffusive Li during subsequent Al deposition)⁴⁴ and may allow the diffusion of oxygen and water into the cell, thereby contributing to device degradation.^{45,46} Methanol solution processed organic cathode interlayers such as PFN⁴⁷ (5 nm thick) and amino-substituted perylene diimide (PDIN)⁴⁸⁻⁵⁰ (methanol solution with 0.2 % acetic acid, 14 nm thick) have also been used to achieve exceptional conventional device performance with relatively longer device stability. For example, Lin *et al.* demonstrated a PCE increase from 5.2 to 6.3 % with improved device stability over time by replacing Ca with PDIN.⁴⁹

The successful cathode work function lowering is attributed to the formation of interface dipoles, and the development of related materials is an active area of research.⁵¹

In inverted high-performance non-fullerene devices, ZnO (20-30 nm thick) is commonly used as an electron transport material interlayer between the BHJ and the ITO cathode. The solution processed ZnO layer is typically spin-coated in the form of nanoparticles⁵² or more often, a sol-gel precursor solution.^{21,34,36,53-56} The ZnO interlayer may be further tuned with the addition of a solution processed fullerene-based self-assembled monolayer (C₆₀-SAM) to passivate electron-trapping hydroxyl groups.^{35,57} Zang *et al.* showed that inverted devices containing the BHJ blend of **PTB7-Th** donor with **di-PDI** discussed above achieved a further improvement in PCE from 5.3 % to 5.9 % through the inclusion of this SAM.³⁵ Li *et al.* reported using a thin layer of ethanolamine to modify the ZnO surface of their inverted devices to achieve the 5.0 % PCE of **PSEHTT:DBFI-T** discussed above.²¹

Poly(3,4-ethylenedioxythiophene): poly(styrene sulphonate) (PEDOT:PSS) is the dominant hole transport material used in conventional non-fullerene small molecule devices.^{21,34,39-43,47-49,58} PEDOT:PSS is typically spin coated to a layer thickness of 30-40 nm onto the ITO anode following UV-ozone cleaning. Despite being acidic, and thereby possibly contributing to device degradation,⁵⁹ PEDOT:PSS is used widely for its superior hole transporting ability.

Transition metal oxides may also act as hole transport materials.⁶⁰ Thermally evaporated MoO_x^{21,34-36,54,56,61} (5-10 nm) is the most prevalent hole transport interlayer employed in high-performance inverted non-fullerene devices, followed by V₂O₅^{55,62,63} (2-20 nm). MoO_x and V₂O₅ are often incorrectly reported to have conduction band minima of -2.3 and -2.4 eV relative to the vacuum level respectively, and work functions of 5.3 and 4.7 eV respectively.^{60,64} UPS and IPES studies have revealed the electron affinity, work function and ionization energy of MoO_x to be 6.7, 6.86, and 9.68 eV respectively,⁶⁵ and those of V₂O₅ to be 6.7, 7.0 and 9.5 eV respectively.⁶⁶ The high work functions and deep lying unoccupied states leads to enhanced hole injection, attributed to electron extraction from the active layer HOMOs into these n-type materials. Although both materials can be solution processed^{67,68} (very recently from Cs-intercalated metal bronze solutions),⁶⁹ in the high-performance devices reported herein, they are generally vacuum deposited followed by an Ag or Al anode.

2.3 Morphology

The vast majority of recent high-performance non-fullerene devices are solution processed from chlorinated solvents such as chloroform (CF), chlorobenzene (CB) and *o*-dichlorobenzene (*o*-DCB), with typical concentrations of ~20 mg/mL for a resulting active layer thickness of ~100 nm. One notable step towards greener solvents was made by Zang *et al.*³⁵ with the use of *o*-xylene. The morphology of BHJ active layers is often tuned to improve device performance in two ways: (1) solvent variation and the inclusion of additives such as DIO and 1-chloronaphthalene (CN)⁷⁰⁻⁷⁴ or solvent blends such as CF mixed with *o*-DCB^{42,54} and (2) through the incorporation of one or more gentle thermal annealing steps (typically 80-120 °C) in the device fabrication procedure.

For example, Holliday *et al.* showed that by using a unique 4:1 CF:*o*-DCB mixture an approximate 1.5-fold increase in PCE was observed when compared to using

the common CB solvent. The D:A ratio is also critical, where the same study revealed significant drops in PCE when moving away from a 1:1 ratio.⁵⁴ Zhong *et al.* demonstrated that the inverted device performance of the 3:7 mass ratio blend of **PTB7** with **Helical PDI** discussed above could be improved beyond 4.5 % PCE through the use of 1 % DIO and 1 % CN solvent additives, achieving a best inverted cell efficiency of 5.2 %.³⁴ On the other hand, Kim *et al.* found that the introduction of 0.5–3.0 % DIO did not improve device performance, but that blended **P3HT** donor and fluorene-based (**Flu-RH**) acceptor devices processed from *o*-DCB outperformed those from CB and CF, at 3.1, 1.3 and 1.3 % respectively.⁵⁸ Zhang *et al.* reported that blends of **PBDTTT-CT** donor with PDI dimer **Bis-PDI-Se-EG** also deteriorate with the inclusion of DIO or CN from a best PCE of 4.0 %, and instead achieved this optimal performance with a unique 6 hour *o*-DCB solvent vapour anneal step.⁷⁵

Heating steps vary from recipe to recipe and may be nuanced; for example, Zhao *et al.* reported heating both the CB blend solution and ITO substrate on a hotplate at 110 °C prior to spin casting, followed by a 5 minute anneal at 100 °C before thermally depositing the top electrode,⁶³ while Singh *et al.* casted from a CF blend solution at 40 °C and anneal for 15 minutes at 100 °C,⁶² and Liu *et al.* heated their CB solution at 110 °C and then annealed for 5 minutes at 80 °C.⁶³ Park and co-workers demonstrated a remarkable increase in PCE from 0.02 % to 5.54 % in an all small-molecule fullerene-free system upon thermally annealing the active layer at 110 °C.⁷⁶ Here, thermal treatment induced phase-separation of the two blended materials resulting in domains suitable for effective charge separation and transport.

A recent review by Liao *et al.* discussed the idealized hierarchical morphology of BHJs as the balance between improving phase separation and suppressing oversized phase separation. AFM and TEM imaging often reveal optimized BHJ films to be relatively smooth with grain sizes typically on the order of tens of nanometers. Non-optimized blend films of the same active materials often have either significantly larger crystallites or amorphous character, and correspondingly poorer device performance.^{36,73,77–79} In addition to processing conditions, the choice of donor and donor/acceptor blend ratio are important factors in device optimization.

3. Donor Considerations

The development of new donor materials, molecular or polymeric, is a rapidly expanding field and has led to a massive quantity of materials with proven photovoltaic potential.^{80–84} The OPV device performance of these materials has generally been evaluated in conjunction with fullerene acceptor materials in the active layer blend, providing a point of comparison for new materials.

Conversely, for the evaluation of non-fullerene acceptors, no comparable “universal donor” exists. In most cases, **P3HT**, the historical standard for donor materials, cannot compare to the efficiencies achieved by active layer blends containing new high performance donor materials that have been developed over the years.^{85,86} For this reason, the importance of selecting an appropriate donor material to assess new non-fullerene acceptors cannot be overstated. Cheng *et al.*⁸⁷ have demonstrated the essential pairing of donor/acceptor materials and its correlation with device performance. This was highlighted by four unique active layer blends where only two of the four realized

appreciable performances, approximately 10-fold increases, in comparison to the other two analogous combinations. Therefore, there are several guidelines to consider when selecting an appropriate material. Optoelectronic compatibility is crucial; most donor materials have been designed with narrow band gaps and thus non-fullerene acceptors can offer a complementary absorption profile to harness higher energy photons. Other considerations include appropriate energy level offset for efficient donor-acceptor charge transfer, as well as active layer thin-film properties where material solubility, crystallinity, and blend morphology each play an important role in realizing high performance.

This review of high performance non-fullerene acceptors reveals that high efficiencies can be achieved by blends with a range of different donor materials and serves to highlight the importance of screening various donor materials to determine the most compatible pairing.

4. Rylene-based Acceptors

Rylene diimide-based π -conjugated materials are among the most efficient polymeric and molecular non-fullerene acceptors to date.⁸⁸ Interest in rylene diimide-based systems results from their innate high electron affinities and mobilities. Coupled with their excellent chemical, thermal and photochemical stability, the ability to tune molecular electronic properties through variation at either the imide nitrogen atoms or the rylene skeleton makes these materials excellent candidates in optoelectronic devices.

Naphthalene diimides (NDIs) have been shown to be effective constituents of several polymeric non-fullerene acceptors,⁸⁹⁻⁹¹ with the best efficiencies to date reaching 5.0 % PCE,⁹² employing an all-polymer active layer composition. Unfortunately, the progress of NDI-based small molecule non-fullerene acceptors has not reached similar heights. To date, the record performance of an electron-accepting small molecule based on the NDI core structure has only reached a best efficiency of 2.4 %.⁹³ Despite their success in polymeric materials, NDI-based small molecule acceptors are not widely studied. On the other hand, perylene diimide, another rylene-type dye, has reached impressive performances as a small molecule non-fullerene acceptor and will be the focus of this section.

Perylene diimides (PDIs) are well-established organic dye molecules with a high electron affinity similar to fullerenes.⁹⁴⁻⁹⁷ They possess large extinction coefficients within the solar spectrum and high electron mobilities. One major obstacle facing PDI derivatives for OPV applications is their tendency to form poor bulk heterojunction morphologies. These extended π -conjugated structures strongly aggregate, leading to crystalline domains that are far too large, in comparison to exciton diffusion lengths (~10 nm), for efficient exciton splitting.^{98,99} Recent synthetic efforts to minimize the formation of such unfavourable domains have focused on the introduction of bulky “swallow tail” branched aliphatic side chains to disrupt the packing structure,^{41,62} often in combination with a twisted PDI material through substitution on the aromatic core.^{40,61,63}

4.1 Monomeric PDI Small Molecules

Linear PDI materials as non-fullerene acceptors have been designed according to the principle that bulky aliphatic side chains or aromatic substitution are sufficient to

promote solubility in common processing solvents for solution processed BHJ OPV devices.

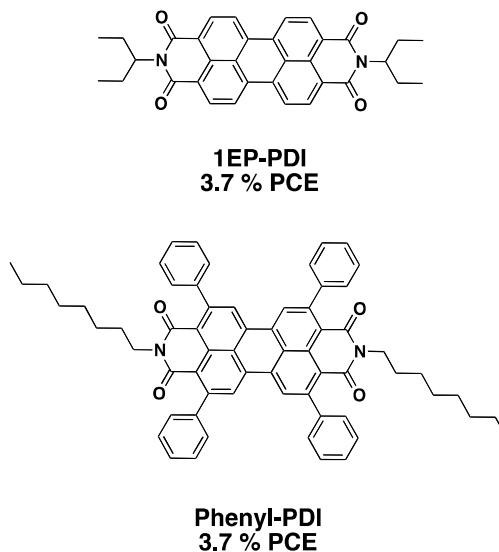


Figure 4.1. Monomeric PDI small molecules

The simplest example of this design methodology for a high performance PDI non-fullerene acceptor is **1EP-PDI** (Figure 4.1), an unsubstituted perylene diimide core functionalized with bulky 1-ethylpropyl side chains. The location of a branching point nearest to the π -conjugated structure sufficiently disrupts the π - π interactions and allows for solubility in organic solvents.^{41,62} **1EP-PDI** offers a broad absorption profile, with maxima at approximately 500 nm and extending beyond 600 nm.¹⁰⁰ The electrochemical properties of the material highlight the inherent π -accepting character of the PDI framework, with an LUMO energy level of approximately -3.8 eV.⁹⁷ The optoelectronic properties of **1EP-PDI** are dictated solely by the PDI chromophore, and serves as an excellent benchmark for comparison with the other PDI-based non-fullerene acceptors discussed in this section. The performance of this non-fullerene acceptor was evaluated in conventional architecture devices in combination with the high performance donor small molecule, *p*-**DTS(FBTTh₂)₂**. These two materials proved to be complementary, with broad spectral coverage (*p*-**DTS(FBTTh₂)₂** absorbing beyond 750 nm) and a LUMO energy offset of 0.5 eV.¹⁰⁰ The optimized devices, processed from chlorobenzene with 0.4 v/v% DIO additive, reached 3.1 % PCE.⁴¹ **1EP-PDI** has also seen success with inverted device architectures. In combination with **PBDTTT-CT**, a donor polymer with similar optoelectronic properties to that of *p*-**DTS(FBTTh₂)₂**, optimized devices with active layers processed from chloroform with 0.4 v/v% DIO additive and a V₂O₅ interlayer between the active layer and the anode reached performances of up to 3.7%.⁶² The addition of small volume fractions of DIO proves to be very important in these examples, providing a means to suppress the formation of large crystalline domains to access a favourable morphology. The high yields and ease of synthetic accessibility coupled with its proven performance highlights **1EP-PDI** as an excellent benchmark

material for screening various donor materials and for comparison with new non-fullerene acceptors.

Another high performance linear PDI acceptor, **Phenyl-PDI** (Figure 4.1), was designed through a high-yielding Ru-catalyzed aromatic substitution with phenyl groups at the “headland” position (C2, C5, C8, and C11). This variation has demonstrated a significant influence on material morphology, leading to a slip-stacked structure, while not completely disrupting the π -stacking. The presence of these substituents also facilitates the solubility of the material in common organic solvents, which can be achieved with simple straight chain octyl aliphatic functionalization, as opposed to the aforementioned branched chains. It was found that the tetrasubstituted PDI core with phenyl groups outperformed those bearing hexyl or phenethyl functionalization, with a red shifted absorption spectrum, stabilization of the energy levels, and moderate thin-film crystallinity. In comparison to **1EP-PDI** the absorption onset of **Phenyl-PDI** remained nearly the same; however, headland phenyl substitution red shifted the absorption maxima by nearly 80 nm, and lowered the LUMO energy level by 0.2 eV. To investigate the photovoltaic performance of **Phenyl-PDI**, active layer devices employed the donor polymer **PBTI3T**,¹⁰¹ and despite its relatively low-lying LUMO energy level of -3.8 eV, proved to be a worthy candidate. **Phenyl-PDI** realized PCEs approaching 3.7 % in an inverted device architecture, optimized with 0.5 v/v% DIO additive.⁶¹

This class of non-fullerene acceptors offers a compelling combination of good photovoltaic performance and simplistic designs accessible from high-yielding and straightforward synthetic procedures. Ultimately, their success serves as a benchmark for the development of more complex PDI acceptors where greater efficiencies have been reached for a number of different structures.

4.2 Non-Linear PDI Small Molecules

Despite the success of simplistic linear PDI materials, the pursuit of high performance PDI materials has been trending towards the development of non-linear PDIs, often consisting of two or more PDI units. The motivation for the design of this class of materials includes the versatility of tailoring different morphologies by molecular design and increased density of states near the LUMO energy. Non-linear PDI materials can be tethered into dimer, trimer or tetramer geometries through carbon-carbon bonds, either directly between PDI units or through a secondary bridging building block.

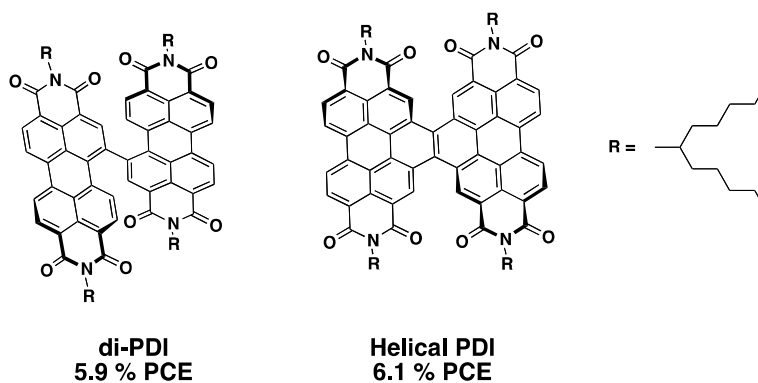


Figure 4.2. Carbon bond tethered dimeric PDI small molecules

The design of **di-PDI** (Figure 4.2), two PDI monomers connected at bay-positions by a single carbon-carbon bond through the Cu-catalyzed homo-coupling of two halogenated PDI monomers, is an excellent introduction to this methodology. This PDI derivative has led to a soluble and flexible structure, a result of a 70° dihedral angle between the two PDI units and imide nitrogen functionalization with symmetrical branched aliphatic side chains. The tethered **di-PDI** material offers more stabilized energy levels than a single PDI unit; however, its spectral coverage is less broad and falls short of 600 nm despite a more than 30 nm red shift in its absorption maxima. It should be noted that this singly-bound PDI dimer yields better OPV device performance than derivatives linked by two or three carbon bonds, which lead to structurally rigid, planar materials.¹⁰² Devices were fabricated in standard conventional and inverted architectures with an **PTB7-Th:di-PDI** active layer blend. The LUMO level of **PTB7** is situated at –3.5 eV, offering a 0.5 eV offset between the two active layer materials. This donor polymer also plays an important role in broadening the spectral coverage, with absorption out to 750 nm and a λ_{max} at 700 nm, well past the λ_{onset} of **di-PDI**. Devices were made to include two processing additives, DIO (1 v/v%) and CN (2 v/v%) and reached efficiencies of 4.2 and 5.3 % respectively. Further device optimization involved the inclusion of ZnO modified self-assembled **PC₆₁BM** monolayer (C₆₀-SAM), and efficiencies rose to 5.9 %.³⁵ Interestingly, **di-PDI** proved to be quite adaptable; it was shown to be processable from *o*-xylenes, a common non-halogenated alternative to chlorobenzene. Devices returned impressive 5.2 % PCEs, while the inclusion of the DIO and CN additives had only marginal effects in the non-halogenated system. The use of this processing solvent is an important feature of this material, where the sustainability of material synthesis, processing, and device fabrication become crucial for eventual large-scale commercial applications.^{103,104} **di-PDI** also proved to be compatible with another high performance donor polymer, **PffBT4T-2DT**.⁵⁵ Benefitting from a smaller LUMO energy offset than **PTB7** (–3.7 eV versus –3.5 eV) devices reached 5.4 % in an inverted architecture employing a V₂O₅ interlayer. This is noteworthy, as a similar trend was not observed for the another PDI acceptor, **SF-PDI₂**, when paired with the same two donor polymers.⁵⁵

A slightly more rigid PDI dimer has exceeded the performance benchmark established by **di-PDI**. The PDI dimer, **Helical PDI** (Figure 4.2), is formed from the photocyclization of two PDI units tethered by an ethylene bridge,¹⁰⁵ and leads to an

approximate 40° twist in the molecular backbone, reducing its propensity to aggregate. Further functionalization with branched aliphatic side chains at the imide nitrogen ensures good solubility in common organic solvents. This alternative tethering of two PDI monomers only slightly raises the LUMO energy level by 0.2 eV to -3.8 eV, but has a much more pronounced influence on the absorption profile. A massive blue shift in the λ_{max} (533 nm versus 390 nm) and a 26 nm blue shift in the absorption onset demonstrates the drastic difference in morphology adopted by **Helical PDI** in comparison to **di-PDI**. An active layer blend with the same donor, **PTB7**, reached initial efficiencies of 3.5 % in a conventional architecture, and 4.5 % in an inverted architecture. Although initially low performance in comparison to **di-PDI**, the substitution of polymeric donor **PTB7** for the slightly less electron-rich analogue **PTB7-Th**, saw the smaller energy offset return efficiencies that reached 6.1 % with co-additives, DIO and CN.³⁴

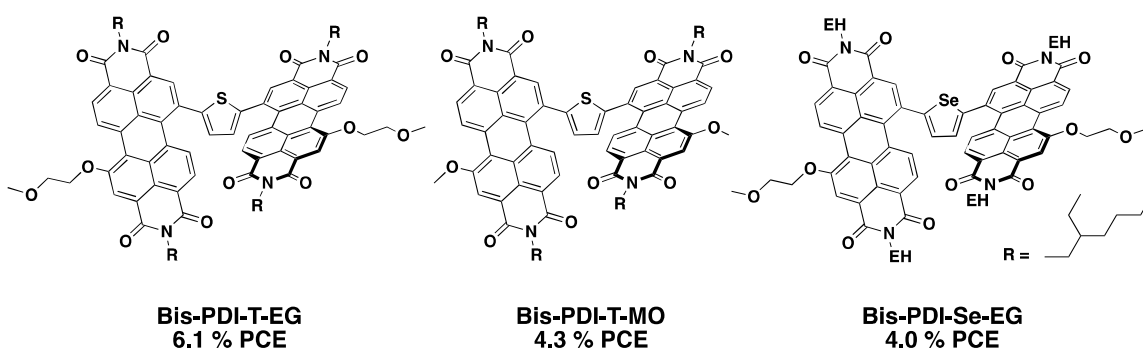


Figure 4.3. Bridged dimeric PDI small molecules.

The incorporation of various bridging units adds to the structural diversity available for linked non-linear PDI materials. **Bis-PDI-T-EG** (Figure 4.3) introduces a thiophene bridging unit between two PDI materials through a Stille reaction protocol, albeit leading to three different isomers of the final material.³⁸ The presence of the bridging thiophene units has a dramatic effect on material conformation, inducing a highly twisted dimeric backbone, with dihedral angles between the planes of 50°–60°. The inclusion of a thiophene bridging unit also had a noticeable influence on the optoelectronic properties of the material. **Bis-PDI-T-EG** exhibited a narrowed band gap in comparison to **di-PDI** (1.9 eV versus 2.1 eV), which translated into a broadened absorption profile, red-shifted by more than 100 nm. This structure bearing aliphatic side chains at the imide nitrogen, as well as ethylene glycol substituents at bay positions, showed adequate solubility in common organic processing solvents. Despite the twisted structure, AFM measurements showed that **Bis-PDI-T-EG** still exhibits strong aggregation and micrometer-sized domains in thin-film blends. Following the incorporation of DIO as a solvent additive, the number of micrometer-sized domains decreased. Improved device performance is attributed to favourable morphology achieved with the DIO additive, as conventional device architectures reached 4.0 % efficiency in combination with the complementary donor polymer **PBDTTT-CT** (0.5 eV LUMO energy offset) but only 0.8 % without the solvent additive. Rigorous optimization of DIO concentration and the use of solvent vapour annealing of the active layer blend led to an

properties of **SF-PDI**₂ are consistent with other materials of this type, exhibiting low-lying LUMO levels similar to that of the thiophene-bridged analogues, but a wider bandgap (2.1 eV versus 1.9 eV) where the HOMO levels are decidedly lower, yet just slightly raised from that of the monomer. As an initial screening, devices were fabricated in an inverted architecture with **P3HT** as the donor component, and reached efficiencies of 2.4 %. Device optimization has since seen the PCE of **SF-PDI**₂ reach 6.3 % in an inverted architecture, which underlines that overall device optimization can lead to substantial performance increases.⁵⁵ Inverted architecture optimization included active layers cast in a 1:1.4 weight ratio from chlorobenzene rather than *o*-dichlorobenzene, and a V₂O₅ interlayer replacing MoO₃. To determine the best energy level compatibility with **SF-PDI**₂ two donor polymers were screened in this evaluation, **PffBT4T-2DT** and **PTB7-Th**. **PffBT4T-2DT**, with the higher-lying LUMO level, reached 6.3 % PCE, in comparison to just 3.0 % for **PTB7-Th**. **PffBT4T-2DT** proved to be more well-matched, with higher J_{sc} values (10.7 versus 7.4 mA cm⁻²) and fill factors (0.57 versus 0.39), potentially due in part to a better active layer morphology with more efficient charge separation and transport. These subtle alterations cannot be overlooked, where variation in device fabrication, active layer processing, and donor selection demonstrates how critical each of these components are to realizing high efficiencies.

The success of PDI-dimer materials has led to the exploration of PDI trimers and tetramers. The introduction of an sp³ hybridized triphenylamine (TPA) central unit *via* a low-yielding (46 %) Suzuki coupling leads to a 3-armed (dendritic) PDI trimer, **S(TPA-PDI)** (Figure 4.5). Dendritic type molecules are attractive for their non-planar structures, which can lead to isotropic optical and charge-transporting properties.⁴⁰ The electron-rich TPA core contributes to the relative high-lying LUMO level of -3.7 eV, the highest energy level of all PDI non-fullerene acceptors discussed in this section. The TPA unit also contributes to the donor-acceptor (D-A) character of the material, effectively narrowing the band gap to 1.8 eV, which is among the smallest for PDI-based non-fullerene acceptors. Solar cell devices using **S(TPA-PDI)** have exhibited performance efficiencies up to 3.3 % in conventional device architecture when paired with one of the more electron-rich donor polymers, **PBDTTT-CT** (0.4 eV energy level offset) and processed from *o*-dichlorobenzene with 5.0 v/v% DIO additive, mitigating aggregation and large domain sizes.

The structure of the high performance 4-arm PDI dendrimer, **TPE-PDI**₄ (Figure 4.5), incorporates a tetraphenylethylene core as the bridging unit between four PDI monomers, accessible through a Suzuki coupling with acceptable yields (63 %). The four phenyl rings of **TPE-PDI**₄ are highly twisted, angled approximately 50° to the double bond, due to steric demand, leading to a propeller-shape structure. In comparison to the 3-arm **S(TPA-PDI)**, LUMO energy levels remain the same; however, the lack of the strong TPA core donor unit reduces the HOMO energy level by approximately 0.3 eV leading to a wide bang gap and blue-shifted absorption profile. Weak intermolecular interactions have been documented for TPE-based materials, leading to excellent solubility in organic solvents even with minimal alkyl side chains. Thin films of **TPE-PDI**₄ have been shown to be smooth and amorphous, with featureless surfaces attributed to the ability of tetraphenylethylene to reduce the aggregation tendency of the PDI units. Devices were fabricated with an inverted architecture using a **PTB7-Th:TPE-PDI**₄ active layer blend and a V₂O₅ anode interlayer. While the absorption profiles of the two

materials complement each other nicely, the energy level offset is among the smallest reported for high performance non-fullerene acceptors with only approximately 0.1 eV between the LUMO of the donor and that of the acceptor. Despite this peculiarity, performance reached PCEs of 5.5 % without any processing additives.⁶³

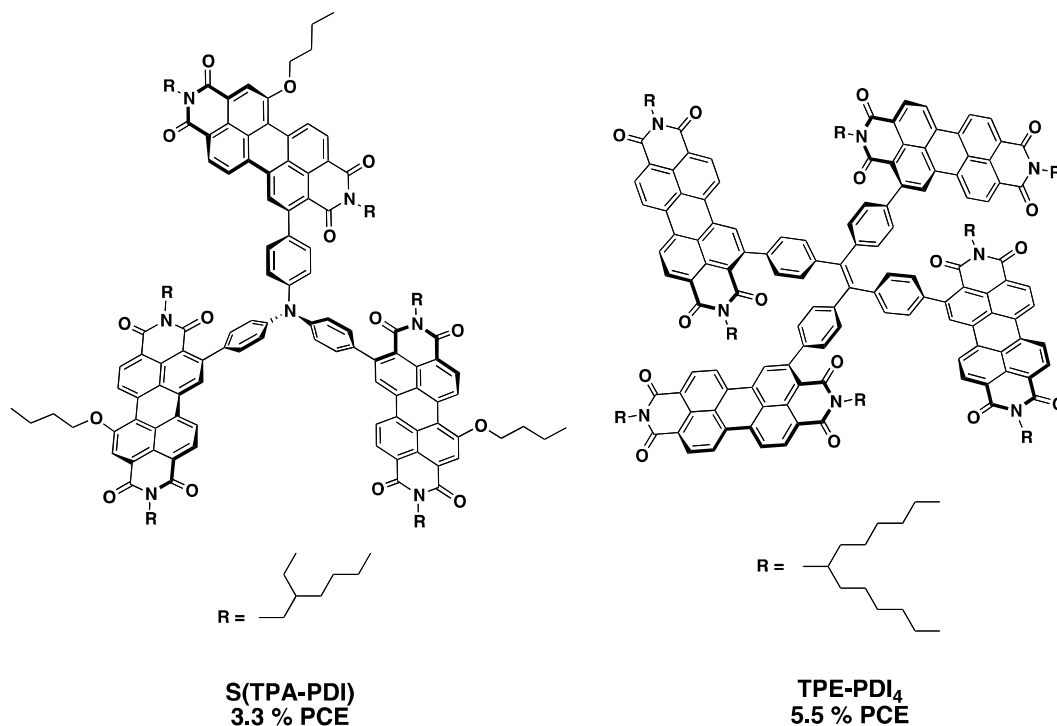


Figure 4.5. Trimeric and tetrameric PDI small molecules.

A summary of key material properties, active layer components and device parameters discussed in this section can be found in Table 4.1 and Table 4.2 respectively. PDI-based materials have reached promising efficiencies and satisfy many of the criteria for a viable alternative to fullerenes as the acceptor component in solution processable BHJ OPV devices, yet these materials still have a few drawbacks. Their aggregation behaviour and crystallinity continue to dictate their molecular design,⁴⁸ often requiring both bulky alkyl side chains and a steric induced twist to the π -conjugated backbone. The synthesis of these materials can be demanding and low yielding with the formation of unwanted isomers, offering little advantage over fullerenes in terms of synthetic scalability.⁵⁴

Table 4.1. Material properties of PDI-based non-fullerene acceptors.

PDI-based Acceptor	HOMO (eV)	LUMO (eV)	Band Gap (eV) ^a	λ_{onset} (nm) ^b	λ_{max} (nm) ^b	Ref
1EP-PDI	-5.8	-3.8	2.0	625*	500*	97
Phenyl-PDI	-6.0	-4.0	2.0	620*	577	61
di-PDI	-6.1	-4.0	2.1	596	533	102

Helical PDI	-6.0	-3.8	2.2	570*	390*	34
Bis-PDI-T-EG	-5.7	-3.8	1.9	706	545	39
Bis-PDI-T-MO	-5.7	-3.8	1.9	680*	540	36
Bis-PDI-Se-EG	-5.6	-3.8	1.8	710*	560*	75
SF-PDI ₂	-5.9	-3.8	2.1	610*	540*	55
S(TPA-PDI)	-5.5	-3.7	1.8	703	536	40
TPE-PDI ₄	-5.8	-3.7	2.1	604	537	63

As material properties are compiled from many different laboratory settings, we caution the reader when comparing these experimental values. Energy levels determined using cyclic voltammetry.

^a Electrochemical band gap

^b Thin-film absorption

* Estimated from absorption spectra

Table 4.2. Active layer materials and device parameters for PDI-based non-fullerene acceptors.

Acceptor	Donor	Architecture	Ratio (D:A)	Processing	Best PCE (%)	Ref
IEP-PDI	PBDTTT-CT	ITO/ZnO/BHJ/V ₂ O ₅ /Ag	3:7	CF + 0.4 v/v% DIO	3.7	41
Phenyl-PDI	PBTI3T	ITO/ZnO/BHJ/MoO ₃ /Ag	1:1	CF + 0.5 v/v% DIO	3.7	61
di-PDI	PTB7-Th	ITO/ZnO/SAM/BHJ/MoO ₃ /Ag	1:1	<i>o</i> -DCB + 1% DIO + 2% CN	5.9	35
Helical PDI	PTB7-Th	ITO/ZnO/BHJ/MoO ₃ /Al	3:7	<i>o</i> -DCB + 1% DIO + 1% CN	6.1	34
Bis-PDI-T-EG	PBDTTT-CT	ITO/PEDOT:PSS/BHJ/Ca/Al	1:1	<i>o</i> -DCB + 1.5% DIO + SVA	6.1	39
Bis-PDI-T-MO	PBDTTT-CT	ITO/ZnO/BHJ/MoO ₃ /Ag	1:1	<i>o</i> -DCB + 2% DIO	4.3	36
Bis-PDI-Se-EG	PBDTTT-CT	ITO/PEDOT:PSS/BHJ/Ca/Al	1:1	<i>o</i> -DCB + SVA	4.0	75
SF-PDI ₂	PffBT4T-2DT	ITO/ZnO/BHJ/V ₂ O ₅ /Al	1:1.4	CB	6.3	55
S(TPA-PDI)	PBDTTT-CT	ITO/PEDOT:PSS/BHJ/Ca/Al	1:1	<i>o</i> -DCB + 5% DIO	3.3	40
TPE-PDI ₄	PTB7-Th	ITO/ZnO/BHJ/V ₂ O ₅ /Al	1:1.4	CB	5.5	63

5. Non-PDI Small Molecule Acceptors

While a large fraction of high performance non-fullerene acceptors are PDI-based, non-PDI small molecules have been designed to be synthetically simple and versatile, with PCEs that can match PDI derivatives. These materials have seen efficiencies rise from 3.0 to nearly 7.0 %, ⁴⁸ surpassing the highest recorded PCE for a PDI-based acceptor this past year.

5.1 Dimeric Small Molecules

Considering the success demonstrated by oligomeric PDI materials, specifically due to their non-planar geometry, several new structures have adopted this methodology as a design principle for new non-PDI small molecule acceptors.

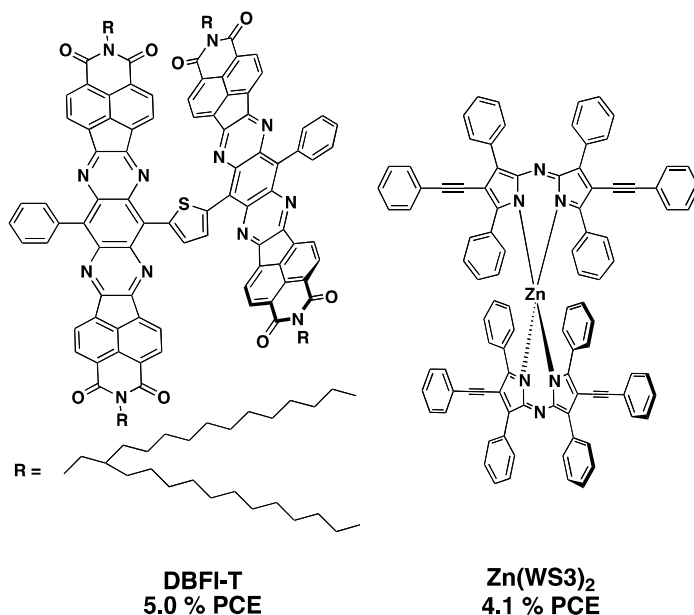


Figure 5.1. Dimeric non-PDI small molecules.

The small molecule dimer, **DBFI-T**,²¹ has a similar design to the thiophene linked PDI dimer **Bis-PDI-T-EG**. Each monomeric unit has a planar and extended π -conjugated core with alkyl functionalized imide moieties to influence solubility, and phenyl substituents to influence intermolecular aggregation. A single thiophene linker is used to bring two monomers together into a dimer conformation, DFT analysis demonstrates that a nearly 33° interplanar angle exists between the two monomeric species due to steric hindrance.²¹ In comparison to the analogous thiophene tethered PDI dimer **Bis-PDI-T-EG**, this rylene-type structure offers nearly identical energy levels but the clear structural differences lead to different absorption profiles with **DBFI-T** offering minimal absorption beyond 450 nm. Employing conventional device architecture, with a LiF cathode interlayer, **DBFI-T** was screened in comparison with its monomeric species and **PC₆₀BM**, blended with a common low-bandgap donor polymer **PSEHTT**,¹⁰⁷ offering a 0.5 eV energy level offset. Due to the negligible absorption of **DBFI-T** beyond 450 nm the spectral coverage of the active layer materials has a large gap between the maxima of **DBFI-T** at 387 nm and that of **PSEHTT** at 579 nm. The thin film morphology was assessed by AFM and displayed uniform nanoscale phase separation with a nearly amorphous surface. When compared to the coarse phase separation of the highly crystalline monomer and its large domain sizes, the importance of the twisted dimeric structure is highlighted, which in this case, led to a favourable film morphology and domain sizes (Figure 5.2). Optimization of the blend active layer composition led to a PCE of 4.2 %, in comparison to 3.6 % achieved by the **PC₆₀BM** blend and more than double that of the monomeric structure blend. Further increases in performance were achieved by switching to the inverted architecture; **DBFI-T** PCEs reached 5.0 %, accompanied by a small efficiency increase for the monomeric material blend, and decrease for the **PC₆₀BM** blend.²¹

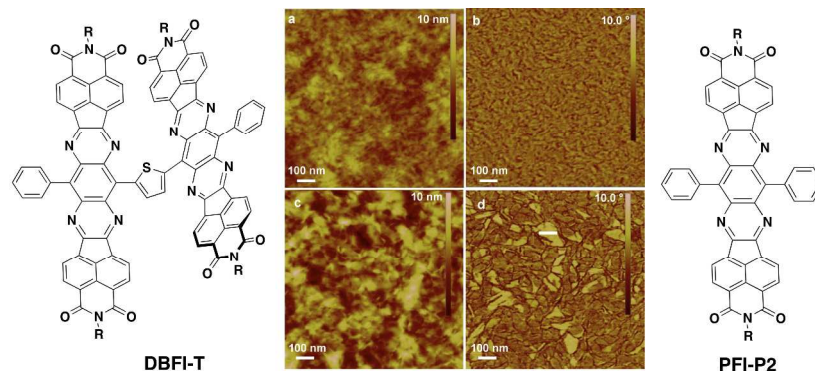


Figure 5.2. AFM surface (a & c) and phase (b & d) images of **PSEHTT:DBFI-T** (a & b) and **PSEHTT:PFI-P2** (c & d) blend films from the best inverted cell. Copyright to be obtained.

Another successful non-planar small molecule has been designed based on an azadipyrromethene dye. These materials have intense absorption in the visible to near-IR region of the solar spectrum and low reduction potentials, and can be further tuned through the coordination of boron or transition metals. Until recent reports, azadipyrromethene materials had not been utilized as electron acceptors for OPVs. The high performance azadipyrromethene-based material **Zn(WS3)₂** has been designed with extended conjugation through the incorporation of phenylethynyl groups at the pyrrolic positions and Zn-coordinated ligands, forming large conjugated structures. **Zn(WS3)₂** is among the most electron-deficient non-PDI fullerene alternatives, with a LUMO energy level of -3.9 eV, on par with many PDI-based materials. As opposed to many of the PDI-based non-fullerene acceptors where λ_{max} is at 500 nm or higher energies, **Zn(WS3)₂** has its maximum absorption approaching 700 nm, which represents one of the most red-shifted λ_{max} for high performance non-fullerene acceptors to date. The twisted nature of these conjugated ligands allows them to point in all directions, potentially resulting in isotropic charge transport while also preventing over-crystallization, leading to favourable nanoscale morphology. The selection of **P3HT** as the donor component in the active layer blend complements the absorption profile of **Zn(WS3)₂**, which resembles many of the high performance donor polymers discussed in this review. In this case, it is the donor component **P3HT**, rather than the acceptor, that offers spectral coverage in the higher energy region, while **Zn(WS3)₂** serves to extend the absorption profile and is responsible for light harvesting in the region of maximum solar flux. The photovoltaic performance of **P3HT:Zn(WS3)₂** active layer blends were investigated in inverted device architectures, and optimized by varying film thickness and thermal annealing conditions, with the best devices reaching 4.1 % PCE.⁵⁶

The successful use of non-planar small molecule acceptors has demonstrated that the methodology of perturbing aggregation by inducing a large twist to the molecular backbones can be extended to non-PDI structures. This represents an important tool for the design of future non-planar small molecules. However, it must be understood that dimeric small molecules are not a necessary criterion for high performance OPV materials.

5.2 Planar Small Molecules

Beyond the well-established performance of both PDI and non-PDI non-planar acceptors, including both PDI and non-PDI materials, linear small molecules as non-fullerene acceptors have also demonstrated impressive OPV device performance.

A common building block for the design of non-fullerene acceptors is benzothiadiazole (BT). BT is a well-known building block used in π -conjugated small molecules for its favourable electron affinity and strong absorption in the visible spectrum¹⁰⁸ when coupled with electron rich units. As such, it comes as no surprise to see BT incorporated in the structure of several high-performance non-fullerene acceptors. **HPI-BT** (Figure 5.3) is an example of a simple BT-based non-fullerene acceptor that has reached impressive performances. **HPI-BT** can be synthesized in a two-step protocol and functionalized with low-cost phthalimide end cap units, another building block that has been incorporated in many electron-accepting materials.^{79,109–113} The synthesis of this material exemplifies the straightforward and versatile synthesis of many non-PDI acceptors, wherein a single synthetic protocol can be adapted to access several materials. **HPI-BT** has one of the widest band-gaps of non-fullerene acceptors at 2.3 eV, with a relatively high lying LUMO level that sits at -3.5 eV. As a result, **HPI-BT** has minimal absorption past 500 nm but contributes to a broad absorption in the high-energy region with maximum absorption at 420 nm. The relatively high-lying LUMO level of **HPI-BT** influences the choice of donor material, where the average LUMO level of the donors discussed in this review rest at -3.5 eV. In this case, **P3HT** was chosen as the donor component, and with a LUMO energy level of -3.2 eV, can offer a suitable energy offset. With the inclusion of **P3HT** the spectral overlap of the active layer extends past 600 nm but remains well short of the broad coverage seen with other non-fullerene acceptors. Initial results demonstrated a 2.5 % efficient device using **P3HT** as the donor,¹⁰⁸ and this has since been improved to reach 3.7 %.⁴³ Much of the performance improvement was attributed to optimization of the synthetic and purification procedures as well as the use of higher purity and regioregularity **P3HT**, highlighting the importance of material purity and its relation to device performance.⁴³

Another high performance non-fullerene acceptor has been designed to incorporate imide-based terminal units. In this case, naphthalimide, a relative of phthalimide, was incorporated.^{76,108,114} **NIDCS-MO** (Figure 5.3) was synthesized through a Stille reaction and a Knoevenagel condensation to incorporate naphthalimide as the end cap unit for a dicyanodistyrylbenzene-based molecular framework.^{115,116} The combination of these building blocks into a functional structure resulted in synergistic electron-accepting properties and complementary self-assembly tendencies. The incorporation of the D-A thiophene-flanked dicyanodistyrylbenzene core unit serves to narrow the band gap of **NIDCS-MO** in comparison to **HPI-BT** lowering the LUMO energy level by 0.2 eV and red-shifting both the λ_{\max} and λ_{onset} . The choice of **p-DTS(FBTTh₂)₂** as the donor material represents an appropriate donor-acceptor pair, highlighted by a 0.4 eV LUMO energy level offset and complementary absorption profile from broad spectral coverage. AFM measurements of the active layer blends with **p-DTS(FBTTh₂)₂** revealed the formation of larger domain sizes upon thermal annealing, yet the films remained reasonably smooth and uniform. The ability to induce small scale morphological changes was exploited in conventional architecture device optimization,

where the fine tuning of annealing conditions and active layer thickness yielded device efficiencies reaching 5.4 %.⁷⁶ This is the best performance for a non-fullerene acceptor with terminal imide acceptors, highlighting the potential for other materials employing similar designs.

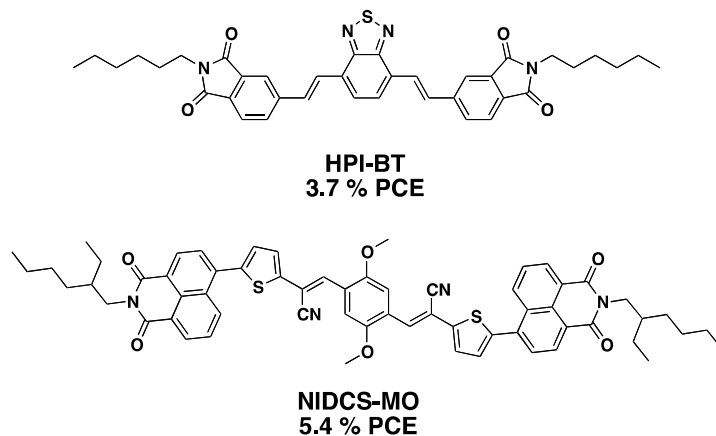


Figure 5.3. Non-fullerene acceptors with terminal imide units.

Several recent high performance non-PDI small molecule acceptors have been built around the common and low-cost building block fluorene. Fluorene offers versatile energy level tuning through substitution at the 2,7 positions and tunable solubility and crystallinity through side-chain engineering. The search for high performance, readily accessible non-fullerene small molecule electron acceptors has been notably pioneered by Watkins *et al.*¹¹⁷ They designed a fluorene-based non-fullerene acceptor assembled using a sustainable and scalable (>20 g) synthetic procedure. Ultimately, OPV performance was low, with the best cell PCE at 2.4 %; however, device optimization rather than material design proved to be the limiting factor in the case of fluorene-based acceptors. **F(DPP)₂B₂** (Figure 5.4) is an excellent example of the inherent capability for high performance of fluorene-based non-fullerene acceptors. **F(DPP)₂B₂** has a thiophene-flanked fluorene core with terminal diketopyrrolopyrrole units, a well-known dye building block.^{111,118,119} Two types of aromatic six-membered rings (fluorene and benzene capped DPP) were chosen as a means to incur small deviations from planarity, achieved through the creation of >20 ° dihedral angles in order to perturb the formation of large aggregates. This DPP-flanked fluorene acceptor employs the D-A approach to band gap engineering, red-shifting the absorption maxima beyond 700 nm; however, this relatively narrow band gap has the most destabilized energy levels of all non-fullerene acceptors reported in this review, with a particularly high LUMO level at -3.4 eV. Similar to **HPI-BT**, the high-lying LUMO level of **F(DPP)₂B₂** has influenced the choice of **P3HT** as the donor component to investigate OPV performance, which is a fitting energy level match and contributes to a broadened the absorption profile in the high-energy region. AFM measurements confirmed the formation of a smooth thin film surface with favourable morphology for OPVs. Device performance was investigated in conventional architecture with a PFN/Al top contact and optimized with thermal annealing. The best efficiency achieved to date for **P3HT:F(DPP)₂B₂** is 3.2 %.⁴⁷

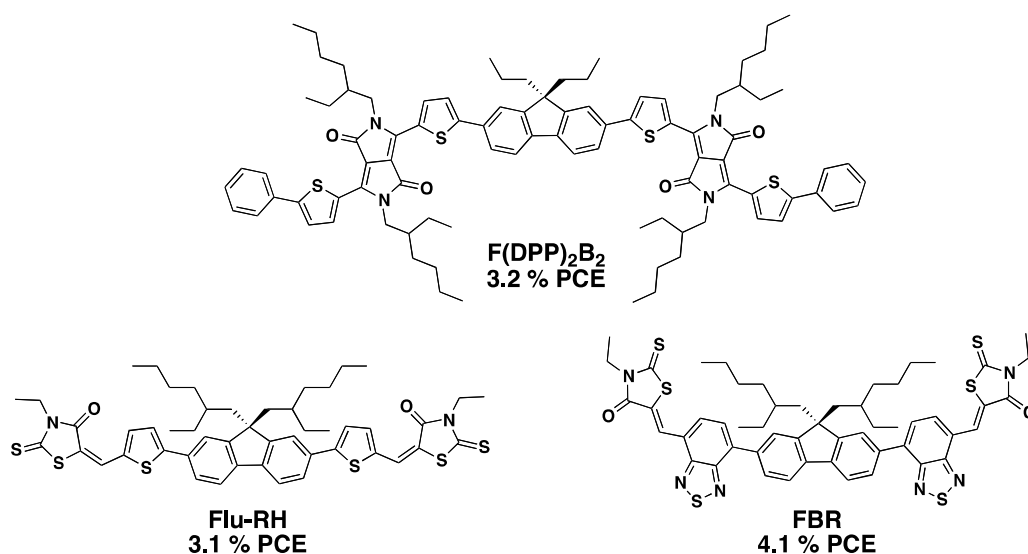


Figure 5.4. Fluorene-based non-PDI small molecules

Flu-RH (Figure 5.4) is another fluorene-based material that has recently surpassed 3.0 % PCE as a non-fullerene acceptor. This material is functionalized with rhodanine end cap units; these building blocks and their derivatives are commonly used in dye chemistry and lead to strong push-pull chromophores, offering electron-withdrawing character through their ketone and thioketone groups. The substitution of these terminal acceptors in place of the ambipolar DPP end caps of **F(DPP)₂B₂** drops the LUMO energy by 0.1 eV, highlighting the more electron-deficient nature of the rhodanine building block. Additional substitution can occur by varying the imide alkyl chain to tailor the solubility of the final material. **Flu-RH** can be synthesized in a sustainable three-step process that makes use of a Suzuki coupling and Knoevenagel condensation, which generate environmentally benign organoboron compounds and water as the respective side products. Similar to **F(DPP)₂B₂**, **Flu-RH** has been investigated as a non-fullerene acceptor with **P3HT** as the donor material. While this active layer composition has a larger energy level offset, the absorption profile of **Flu-RH** is very similar to that of **P3HT** ($\lambda_{\text{max}} = 510 \text{ nm}$, 550 nm and $\lambda_{\text{onset}} = 600 \text{ nm}$, 650 nm respectively) and therefore does not offer the broad coverage seen for **P3HT:F(DPP)₂B₂**. AFM measurements of the active layer morphology highlighted the influence of processing solvent; where roughness was found to increase in active layers cast from *o*-dichlorobenzene in comparison to chloroform. Consequently, device optimization included assessment of processing solvents and thermal annealing temperatures. As a result, the performance of **Flu-RH** peaked at 3.1 % when cast from *o*-dichlorobenzene compared to 1.3 % from chloroform.⁵⁸ Ultimately **F(DPP)₂B₂** and **Flu-RH** returned similar efficiencies; however, structural modification of the **Flu-RH** framework eventually led to the highest performance fluorene-based non-fullerene acceptor to date.

FBR (Figure 5.4) has a related structure to **Flu-RH**, and has improved on the established efficiencies of its predecessor. Modification to the structure of **Flu-RH** occurs at the thiophene bridge, replacing this weak donor with an electron-deficient BT

substituent. **FBR** is synthesized through a similar protocol to that outlined for **Flu-RH**, highlighting the versatility of such a molecular architecture. The replacement of thiophene with BT dropped the HOMO and LUMO energy levels by 0.1 eV but band gap remained the same, with a slight blue-shift in the onset of absorption. To evaluate the performance of this material, devices were fabricated in an inverted architecture with **P3HT** as the donor material, and led to no discernable thin film aggregation based on optical microscope images of the active blends. In comparison to **Flu-RH**, **FBR** has a larger LUMO energy offset with the **P3HT** donor; however, it appears that thin-film morphology was more influential on device performance. The reported thin-film roughness of **P3HT:Flu-RH** did not manifest in thin-films of **P3HT:FBR**, presumably due to the different self-assembly tendencies resulting from thiophene for BT substitution. Optimization of devices included active layer thickness, post-deposition thermal annealing and a 4:1 CHCl_3 :*o*-DCB processing solvent mixture. Device performance has reached 4.1 % PCE, which is among the highest efficiencies for a non-fullerene based device with **P3HT**.⁵⁴

Indacenodithiophene-based π -conjugated materials are another promising class of non-fullerene acceptors. The indacenodithiophene unit is a rigid and planar structure with excellent hole transporting and light absorption properties.¹²⁰⁻¹²² This five-ring fused core can be substituted with four rigid *p*-hexylphenyl groups to restrict molecular planarity, aggregation tendency and thus the formation of large domain sizes in BHJ active layer blends. Investigation of these materials as potential non-fullerene acceptors has focused on incorporating strong electron-withdrawing terminal units to tune the energy levels in order to provide a suitable energy offset when paired with established donor materials.

DC-IDT2T (Figure 5.5) is an excellent example of this methodology put into practice. Through the incorporation of strong electron-withdrawing dicyanomethylene-indanone end cap units bearing one carbonyl and two cyano groups, the electron affinity of the material is drastically increased, making it suitable for accepting electrons. The material can be synthesized in high yields in two synthetic steps, where the precursor to the final material has terminal aldehyde units enabling various end cap units to be installed *via* Knoevenagel condensations. **DC-IDT2T** is a narrow band gap non-fullerene acceptor with broad optical absorption from 600 to 800 nm. Its low-lying LUMO level at -3.9 eV is comparable to the values for many of the PDI-based acceptors. To demonstrate the potential of **DC-IDT2T** as a non-fullerene acceptor, devices were fabricated with the conventional architecture and optimized with respect to weight ratios and the use of co-solvents to modify and control the morphology of the active layer. A dichlorobenzene and chloroform (15 v/v%) processing solvent combination was used to deposit active layer films of **PBDTTT-CT:DC-IDT2T** and led to a smooth morphology where AFM images suggested the presence of favourable interpenetrating networks without detrimental phase separation. The **PBDTTT-CT:DC-IDT2T** active layer blend has an energy level offset of 0.6 eV and constitutes one of the largest reported offsets for high performance non-fullerene acceptors. This active layer composition and its strong optical absorption in the region of maximum solar flux returned an OPV device performance best cell PCE of 3.9 % without any post-deposition treatment.⁴²

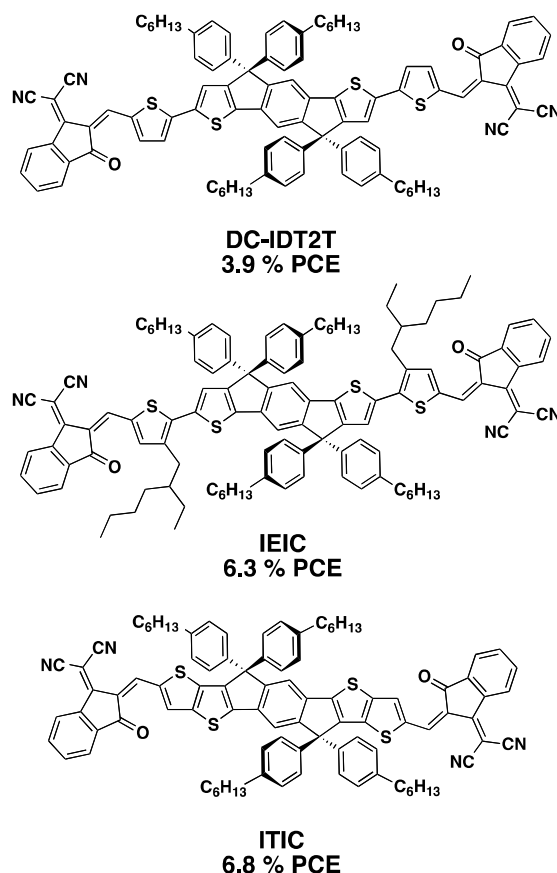


Figure 5.5. Indacenodithiophene-based non-fullerene acceptors.

Building on this established success, a derivative of **DC-IDT2T** was synthesized based on the same molecular framework to include 2-ethylhexyl side chains substituted at each of the 3-positions of the thiophene bridge, contributing to material solubility and aggregation behaviour. This structural modification had no significant influence on the optoelectronic properties of the material and instead targeted a more favourable thin-film morphology through altered self-assembly tendencies as a result of the additional branch alkyl chains. The device performance of **IEIC** (Figure 5.5) was assessed in a conventional architecture, with the high performance polymer **PTB7-Th** instead of **PBDTTT-CT**, contributing to stronger light absorption in the 700–800 nm region. **PTB7-Th** offers a 0.3 eV lower LUMO energy level than **PBDTTT-CT**, drastically reducing the large energetic loss associated with the 0.6 eV offset of **PBDTTT-CT:DC-IDT2T**. Device fabrication was optimized for weight ratios, leading to a smooth morphology with nearly uniform crystalline domains. Initial OPV device performance reached 5.2 % and later rose to 6.3 % through the addition of an PDIN interlayer between the active layer and the top contact.⁴⁹

The highest performance non-fullerene acceptor to date is another structural derivative of **DC-IDT2T**, in which the thiophene bridge has been incorporated into the core as a fused bithiophene unit, leading to a seven-ring core structure. **ITIC** (Figure 5.5), adopts essentially the same electrochemical properties as its predecessors with a slight blue shift in both the maximum and onset of absorption. Devices were fabricated in a

similar fashion to that of **IEIC**, employing a conventional device architecture with a **PDIN** interlayer and **PTB7-Th** as the donor polymer. The active layer morphology, as determined by AFM, was smooth, showing good miscibility of blend materials with uniform crystalline domains. The fused seven ring system clearly promoted the formation of a favourable active layer morphology as PCEs for the **PTB7-Th:ITIC** active layer reached 6.8 %, representing the highest PCE of a non-fullerene to date.⁴⁸

A summary of key material properties, as well as active layer components and device parameters discussed in this section can be found in Table 5.1 and Table 5.2 respectively. As communicated, the development of small molecule non-fullerene acceptors has resulted in an excellent progression in OPV performance. This highlights the potential of these materials, offering comparable efficiencies to commonly used PDI acceptors with an advantage in terms of a low-cost, versatile, high-yielding and scalable synthetic accessibility.

Table 5.1. Material properties of small molecule non-fullerene acceptors.

Non-Fullerene Acceptor	HOMO (eV)	LUMO (eV)	Band Gap (eV) ^a	λ_{onset} (nm) ^b	λ_{max} (nm) ^b	Ref
DBFI-T	-5.8	-3.8	2.0	675*	387	21
Zn(WS3)₂	-5.6	-3.9	1.7	800	696	56
HPI-BT	-5.8	-3.5	2.3	540*	420*	108
NIDCS-MO	-5.8	-3.7	2.1	620*	498	76
F(DPP)₂B₂	-5.2	-3.4	1.8	710*	650*	47
Flu-RH	-5.6	-3.5	2.1	600*	510	58
FBR	-5.7	-3.6	2.1	560*	509	54
DC-IDT2T	-5.4	-3.9	1.5	800	720	42
IEIC	-5.4	-3.8	1.6	790	722	49
ITIC	-5.5	-3.8	1.7	780	702	48

As material properties are compiled from many different laboratory settings, we caution the reader when comparing these experimental values. Energy levels determined using cyclic voltammetry.

^a Electrochemical band gap

^b Thin-film absorption

* Estimated from absorption spectra

Table 5.2. Active layer materials and device parameters for small molecule non-fullerene acceptors.

Acceptor	Donor	Architecture	Ratio (D:A)	Processing	Best PCE (%)	Ref
DBFI-T	PSEHTT	ITO/ZnO/BHJ/MoO ₃ /Ag	1:2	CF	5.0	21
Zn(WS3)₂	P3HT	ITO/ZnO/BHJ/MoO ₃ /Ag	1:0.7	<i>o</i> -DCB	4.1	56
HPI-BT	P3HT	ITO/PEDOT:PSS/BHJ/LiF/Al	1:2	CB	3.7	108
NIDCS-MO	<i>p</i>-DTS(FBTTh₂)₂	ITO/PEDOT:PSS/BHJ/Ca/Al	1:1	CF	5.4	76
F(DPP)₂B₂	P3HT	ITO/PEDOT:PSS/BHJ/PFN/Al	1:1	CF	3.2	47
Flu-RH	P3HT	ITO/PEDOT:PSS/BHJ/LiF/Al	1:1.5	<i>o</i> -DCB	3.1	58
FBR	P3HT	ITO/ZnO/BHJ/MoO ₃ /Ag	1:1	CF: <i>o</i> -DCB (1:4)	4.1	54

DC-IDT2T	PBDTTT-CT	ITO/PEDOT:PSS/BHJ/Ca/Al	1.2:1	<i>o</i> -DCB + 15% CF	3.9	42
IEIC	PTB7-Th	ITO/PEDOT:PSS/BHJ/PDIN/Al	1:1.5	<i>o</i> -DCB	6.3	49
ITIC	PTB7-Th	ITO/PEDOT:PSS/BHJ/PDIN/Al	1:1.3	<i>o</i> -DCB	6.8	48

6. Conclusions

The versatility of π -conjugated small molecule acceptors has enabled the fine-tuning of material properties through structural modification and has led to the emergence of a large diversity of materials in the development of alternatives to fullerene acceptors in OPV devices.

While the diversity of the high-performance non-fullerene acceptors reviewed herein cannot be understated, the reader should be aware of the three common design themes: (1) strong electron-withdrawing functionalities to increase the π -accepting character of the molecular framework (2) bulky substituents and induced non-planarity to reduce the propensity for strong π - π interactions and large aggregate formation, (3) aliphatic side chains to promote material solubility and influence thin-film morphology. The successful implementation of these design strategies with the help of significant advances in device optimization have led to remarkable improvements in device performance where the benchmark materials have risen from 3 to nearly 7 % efficiencies within the last year. Yet, despite this noted success, one must realize these non-fullerene acceptors are often limited to high efficiencies with only one specific donor material, unlike fullerene derivatives, which have been shown to be compatible with a range of donors. This raises the question are these efficiencies an effect of the non-fullerene acceptor or are they primarily a consequence of the established high-performance donor material? Therefore, the challenge remains to find a non-fullerene acceptor that can achieve high performance with a range of donor materials.

In particular, significant advancement in the development of all-small-molecule BHJ devices is required to take advantage of the well-known benefits of molecular over polymeric systems. This is highlighted by the fact that the composition of the majority of high-performance active layer blends includes a polymeric donor, and only two of the twenty device architectures we have reviewed make use of a molecular donor. Evidently, high-performance all-small-molecule active layers have proved to be significantly challenging. This should encourage their investigation in the interest of further progress in non-fullerene acceptors for OPVs.

Notes and Acknowledgments

Chemical structures of donor materials and interlayers are given in the Supporting Information.

We thank Liz Kitching for contributing the device schematic figure concept. GCW acknowledges the NSERC Discovery Program, Canada Research Chairs, and the Canadian Foundation for Innovation. IGH acknowledges the NSERC Discovery Program and NSERC Photovoltaics Innovation Network. JMT acknowledges NSERC CREATE DREAMS for salary support.

References

- 1 S. B. Darling and F. You, *RSC Adv.*, 2013, **3**, 17633–17648.
- 2 S. R. Forrest, *Nature*, 2004, **428**, 911–918.
- 3 M. Kaltenbrunner, M. S. White, E. D. Glowacki, T. Sekitani, T. Someya, N. S. Sariciftci and S. Bauer, *Nat. Commun.*, 2012, **3**, 770–777.
- 4 B. Kippelen and J.-L. Brédas, *Energy Environ. Sci.*, 2009, **2**, 251–261.
- 5 G. Li, R. Zhu and Y. Yang, *Nat. Photonics*, 2012, **6**, 153–161.
- 6 R. Søndergaard, M. Hösel, D. Angmo, T. T. Larsen-Olsen and F. C. Krebs, *Mater. Today*, 2012, **15**, 36–49.
- 7 Y.-W. Su, S.-C. Lan and K.-H. Wei, *Mater. Today*, 2012, **15**, 554–562.
- 8 G. Dennler, M. C. Scharber and C. J. Brabec, *Adv. Mater.*, 2009, **21**, 1323–1338.
- 9 D. Gendron and M. Leclerc, *Energy Environ. Sci.*, 2011, **4**, 1225–1237.
- 10 C. Duan, F. Huang and Y. Cao, *J. Mater. Chem.*, 2012, **22**, 10416–10434.
- 11 J. Roncali, *Acc. Chem. Res.*, 2009, **42**, 1719–1730.
- 12 J. Roncali, P. Leriche and P. Blanchard, *Adv. Mater.*, 2014, **26**, 3821–3838.
- 13 A. Mishra and P. Bäuerle, *Angew. Chem. Int. Ed.*, 2012, **51**, 2020–2067.
- 14 A. F. Eftaiha, J.-P. Sun, I. G. Hill and G. C. Welch, *J. Mater. Chem. A*, 2013, **2**, 1201–1213.
- 15 Y. Lin and X. Zhan, *Mater. Horiz.*, 2014, **1**, 470–488.
- 16 P. Sonar, J. P. F. Lim and K. L. Chan, *Energy Environ. Sci.*, 2011, **4**, 1558–1574.
- 17 E. Kozma and M. Catellani, *Dyes Pigments*, 2013, **98**, 160–179.
- 18 J. E. Anthony, *Chem. Mater.*, 2011, **23**, 583–590.
- 19 C. L. Chochos, N. Tagmatarchis and V. G. Gregoriou, *RSC Adv.*, 2013, **3**, 7160–7181.
- 20 P. Hudhomme, *EPJ Photovolt.*, 2013, **4**, 40401–40412.
- 21 H. Li, T. Earmme, G. Ren, A. Saeki, S. Yoshikawa, N. M. Murari, S. Subramaniyan, M. J. Crane, S. Seki and S. A. Jenekhe, *J. Am. Chem. Soc.*, 2014, **136**, 14589–14597.
- 22 T. Liu and A. Troisi, *Adv. Mater.*, 2013, **25**, 1038–1041.
- 23 Y. Kanai and J. C. Grossman, *Nano Lett.*, 2007, **7**, 1967–1972.
- 24 T. W. Holcombe, J. E. Norton, J. Rivnay, C. H. Woo, L. Goris, C. Piliago, G. Griffini, A. Sellinger, J.-L. Brédas, A. Salleo and J. M. J. Fréchet, *J. Am. Chem. Soc.*, 2011, **133**, 12106–12114.
- 25 R. D. Pensack, C. Guo, K. Vakhshouri, E. D. Gomez and J. B. Asbury, *J. Phys. Chem. C*, 2012, **116**, 4824–4831.
- 26 B. M. Savoie, A. Rao, A. A. Bakulin, S. Gelinas, B. Movaghar, R. H. Friend, T. J. Marks and M. A. Ratner, *J. Am. Chem. Soc.*, 2014, **136**, 2876–2884.
- 27 A. A. Bakulin, A. Rao, V. G. Pavelyev, P. H. M. van Loosdrecht, M. S. Pshenichnikov, D. Niedzialek, J. Cornil, D. Beljonne and R. H. Friend, *Science*, 2012, **335**, 1340–1344.
- 28 M. D. Perez, C. Borek, S. R. Forrest and M. E. Thompson, *J. Am. Chem. Soc.*, 2009, **131**, 9281–9286.
- 29 S. R. Cowan, N. Banerji, W. L. Leong and A. J. Heeger, *Adv. Funct. Mater.*, 2012, **22**, 1116–1128.
- 30 B. A. Gregg, *J. Phys. Chem. Lett.*, 2011, **2**, 3013–3015.
- 31 J. Roncali, P. Leriche and A. Cravino, *Adv. Mater.*, 2007, **19**, 2045–2060.

- 32 A. L. Kanibolotsky, I. F. Perepichka and P. J. Skabara, *Chem. Soc. Rev.*, 2010, **39**, 2695–2728.
- 33 F. Huang, H. Wu, D. Wang, W. Yang and Y. Cao, *Chem. Mater.*, 2004, **16**, 708–716.
- 34 Y. Zhong, M. T. Trinh, R. Chen, W. Wang, P. P. Khlyabich, B. Kumar, Q. Xu, C.-Y. Nam, M. Y. Sfeir, C. Black, M. L. Steigerwald, Y.-L. Loo, S. Xiao, F. Ng, X.-Y. Zhu and C. Nuckolls, *J. Am. Chem. Soc.*, 2014, **136**, 15215–15221.
- 35 Y. Zang, C.-Z. Li, C.-C. Chueh, S. T. Williams, W. Jiang, Z.-H. Wang, J.-S. Yu and A. K.-Y. Jen, *Adv. Mater.*, 2014, **26**, 5708–5714.
- 36 Z. Lu, B. Jiang, X. Zhang, A. Tang, L. Chen, C. Zhan and J. Yao, *Chem. Mater.*, 2014, **26**, 2907–2914.
- 37 T.-H. Lai, S.-W. Tsang, J. R. Manders, S. Chen and F. So, *Mater. Today*, 2013, **16**, 424–432.
- 38 X. Zhang, Z. Lu, L. Ye, C. Zhan, J. Hou, S. Zhang, B. Jiang, Y. Zhao, J. Huang, S. Zhang, Y. Liu, Q. Shi, Y. Liu and J. Yao, *Adv. Mater.*, 2013, **25**, 5791–5797.
- 39 X. Zhang, C. Zhan and J. Yao, *Chem. Mater.*, 2014, **27**, 166–173.
- 40 Y. Lin, Y. Wang, J. Wang, J. Hou, Y. Li, D. Zhu and X. Zhan, *Adv. Mater.*, 2014, **26**, 5137–5142.
- 41 A. Sharenko, D. Gehrig, F. Laquai and T.-Q. Nguyen, *Chem. Mater.*, 2014, **26**, 4109–4118.
- 42 H. Bai, Y. Wang, P. Cheng, J. Wang, Y. Wu, J. Hou and X. Zhan, *J. Mater. Chem. A*, 2014, **3**, 1910–1914.
- 43 J. T. Bloking, T. Giovenzana, A. T. Higgs, A. J. Ponc, E. T. Hoke, K. Vandewal, S. Ko, Z. Bao, A. Sellinger and M. D. McGehee, *Adv. Energy Mater.*, 2014, **4**, 1301426(1)–1301426(12).
- 44 J. U. Lee, J. W. Jung, J. W. Jo and W. H. Jo, *J. Mater. Chem.*, 2012, **22**, 24265–24283.
- 45 N. Grossiord, J. M. Kroon, R. Andriessen and P. W. M. Blom, *Org. Electron.*, 2012, **13**, 432–456.
- 46 F. C. Krebs and K. Norrman, *Prog. Photovolt. Res. Appl.*, 2007, **15**, 697–712.
- 47 H. Shi, W. Fu, M. Shi, J. Ling and H. Chen, *J. Mater. Chem. A*, 2015, **3**, 1902–1905.
- 48 Y. Lin, J. Wang, Z.-G. Zhang, H. Bai, Y. Li, D. Zhu and X. Zhan, *Adv. Mater.*, 2015, **27**, 1170–1174.
- 49 Y. Lin, Z.-G. Zhang, H. Bai, J. Wang, Y. Yao, Y. Li, D. Zhu and X. Zhan, *Energy Environ. Sci.*, 2014, **8**, 610–616.
- 50 S. Kundu, S. R. Gollu, R. Sharma, S. G. A. Ashok, A. R. Kulkarni and D. Gupta, *Org. Electron.*, 2013, **14**, 3083–3088.
- 51 Y. Zhang, Z. F. Zhao, J. B. He, J. Wang, W. Chen, N. Wang and R. Yang, *J. Mater. Chem. C*, 2015, **3**, 4514–4521.
- 52 J. Jo, J.-R. Pouliot, D. Wynands, S. D. Collins, J. Y. Kim, T. L. Nguyen, H. Y. Woo, Y. Sun, M. Leclerc and A. J. Heeger, *Adv. Mater.*, 2013, **25**, 4783–4788.
- 53 Y. Sun, J. H. Seo, C. J. Takacs, J. Seifter and A. J. Heeger, *Adv. Mater.*, 2011, **23**, 1679–1683.
- 54 S. Holliday, R. S. Ashraf, C. B. Nielsen, M. Kirkus, J. A. Röhr, C.-H. Tan, E. Collado-Fregoso, A.-C. Knall, J. R. Durrant, J. Nelson and I. McCulloch, *J. Am. Chem. Soc.*, 2014, **137**, 898–904.
- 55 J. Zhao, Y. Li, H. Lin, Y. Liu, K. Jiang, C. Mu, T. Ma, J. Y. L. Lai, H. Hu, D. Yu

- and H. Yan, *Energy Environ. Sci.*, 2015, **8**, 520–525.
- 56 Z. Mao, W. Senevirathna, J.-Y. Liao, J. Gu, S. V. Kesava, C. Guo, E. D. Gomez and G. Sauv e, *Adv. Mater.*, 2014, **26**, 6290–6294.
- 57 S. K. Hau, H.-L. Yip, H. Ma and A. K.-Y. Jen, *Appl. Phys. Lett.*, 2008, **93**, 233304.
- 58 Y. Kim, C. E. Song, S.-J. Moon and E. Lim, *Chem. Commun.*, 2014, **50**, 8235–8238.
- 59 H. Choi, H.-B. Kim, S.-J. Ko, J. Y. Kim and A. J. Heeger, *Adv. Mater.*, 2015, **27**, 892–896.
- 60 V. Shrotriya, G. Li, Y. Yao, C.-W. Chu and Y. Yang, *Appl. Phys. Lett.*, 2006, **88**, 073508(1)–073508(3).
- 61 P. E. Hartnett, A. Timalina, H. S. S. R. Matte, N. Zhou, X. Guo, W. Zhao, A. Facchetti, R. P. H. Chang, M. C. Hersam, M. R. Wasielewski and T. J. Marks, *J. Am. Chem. Soc.*, 2014, **136**, 16345–16356.
- 62 R. Singh, E. Aluicio-Sarduy, Z. Kan, T. Ye, R. C. I. MacKenzie and P. E. Keivanidis, *J. Mater. Chem. A*, 2014, **2**, 14348–14353.
- 63 Y. Liu, C. Mu, K. Jiang, J. Zhao, Y. Li, L. Zhang, Z. Li, J. Y. L. Lai, H. Hu, T. Ma, R. Hu, D. Yu, X. Huang, B. Z. Tang and H. Yan, *Adv. Mater.*, 2014, **27**, 1015–1020.
- 64 R. Po, C. Carbonera, A. Bernardi and N. Camaioni, *Energy Environ. Sci.*, 2011, **4**, 285–310.
- 65 M. Kr ger, S. Hamwi, J. Meyer, T. Riedl, W. Kowalsky and A. Kahn, *Appl. Phys. Lett.*, 2009, **95**, 123301(1)–123301(3).
- 66 J. Meyer, K. Zilberberg, T. Riedl and A. Kahn, *J. Appl. Phys.*, 2011, **110**, 033710(1)–033710(3).
- 67 C. Girotto, E. Voroshazi, D. Cheyns, P. Heremans and B. P. Rand, *ACS Appl. Mater. Interfaces*, 2011, **3**, 3244–3247.
- 68 K. Zilberberg, S. Trost, H. Schmidt and T. Riedl, *Adv. Energy Mater.*, 2011, **1**, 377–381.
- 69 X. Li, F. Xie, S. Zhang, J. Hou and W. C. Choy, *Light Sci. Appl.*, 2015, **4**, e273(1)–e273(7).
- 70 J. K. Lee, W. L. Ma, C. J. Brabec, J. Yuen, J. S. Moon, J. Y. Kim, K. Lee, G. C. Bazan and A. J. Heeger, *J. Am. Chem. Soc.*, 2008, **130**, 3619–3623.
- 71 X. Guo, C. Cui, M. Zhang, L. Huo, Y. Huang, J. Hou and Y. Li, *Energy Environ. Sci.*, 2012, **5**, 7943–7949.
- 72 C. V. Hoven, X.-D. Dang, R. C. Coffin, J. Peet, T.-Q. Nguyen and G. C. Bazan, *Adv. Mater.*, 2010, **22**, E63–E66.
- 73 H.-C. Liao, C.-C. Ho, C.-Y. Chang, M.-H. Jao, S. B. Darling and W.-F. Su, *Mater. Today*, 2013, **16**, 326–336.
- 74 L. Chang, I. E. Jacobs, M. P. Augustine and A. J. Moul e, *Org. Electron.*, 2013, **14**, 2431–2443.
- 75 X. Zhang, J. Yao and C. Zhan, *Chem. Commun.*, 2014, **51**, 1058–1061.
- 76 O. K. Kwon, J.-H. Park, D. W. Kim, S. K. Park and S. Y. Park, *Adv. Mater.*, 2015, **27**, 1951–1956.
- 77 J. A. Love, C. M. Proctor, J. Liu, C. J. Takacs, A. Sharenko, T. S. van der Poll, A. J. Heeger, G. C. Bazan and T.-Q. Nguyen, *Adv. Funct. Mater.*, 2013, **23**, 5019–5026.
- 78 J. R. Tumbleston, B. A. Collins, L. Yang, A. C. Stuart, E. Gann, W. Ma, W. You and H. Ade, *Nat. Photonics*, 2014, **8**, 385–391.
- 79 S. M. McAfee, J. M. Toppie, A.-J. Payne, J.-P. Sun, I. G. Hill and G. C. Welch,

- ChemPhysChem*, 2015, **16**, 1190–1202.
- 80 J. E. Coughlin, Z. B. Henson, G. C. Welch and G. C. Bazan, *Acc. Chem. Res.*, 2014, **47**, 257–270.
- 81 F. Zhang, D. Wu, Y. Xu and X. Feng, *J. Mater. Chem.*, 2011, **21**, 17590–17600.
- 82 B. Walker, C. Kim and T.-Q. Nguyen, *Chem. Mater.*, 2011, **23**, 470–482.
- 83 Y. Lin, Y. Li and X. Zhan, *Chem. Soc. Rev.*, 2012, **41**, 4245–4272.
- 84 Y. Chen, X. Wan and G. Long, *Acc. Chem. Res.*, 2013, **46**, 2645–2655.
- 85 L. Dou, J. You, Z. Hong, Z. Xu, G. Li, R. A. Street and Y. Yang, *Adv. Mater.*, 2013, **25**, 6642–6671.
- 86 H. J. Son, F. He, B. Carsten and L. Yu, *J. Mater. Chem.*, 2011, **21**, 18934–18945.
- 87 P. Cheng, X. Zhao, W. Zhou, J. Hou, Y. Li and X. Zhan, *Org. Electron.*, 2014, **15**, 2270–2276.
- 88 X. Zhan, A. Facchetti, S. Barlow, T. J. Marks, M. A. Ratner, M. R. Wasielewski and S. R. Marder, *Adv. Mater.*, 2011, **23**, 268–284.
- 89 A. Facchetti, *Mater. Today*, 2013, **16**, 123–132.
- 90 Y.-J. Hwang, T. Earmme, B. A. E. Courtright, F. N. Eberle and S. A. Jenekhe, *J. Am. Chem. Soc.*, 2015, **137**, 4424–4434.
- 91 T. Earmme, Y.-J. Hwang, N. M. Murari, S. Subramaniam and S. A. Jenekhe, *J. Am. Chem. Soc.*, 2013, **135**, 14960–14963.
- 92 C. Mu, P. Liu, W. Ma, K. Jiang, J. Zhao, K. Zhang, Z. Chen, Z. Wei, Y. Yi, J. Wang, S. Yang, F. Huang, A. Facchetti, H. Ade and H. Yan, *Adv. Mater.*, 2014, **26**, 7224–7230.
- 93 Y. Liu, L. Zhang, H. Lee, H.-W. Wang, A. Santala, F. Liu, Y. Diao, A. L. Briseno and T. P. Russell, *Adv. Energy Mater.*, 2015, 1500195(1)–1500195(8).
- 94 L. Schmidt-Mende, A. Fechtenkötter, K. Müllen, E. Moons, R. H. Friend and J. D. MacKenzie, *Science*, 2001, **293**, 1119–1122.
- 95 J. H. Schön, C. Kloc and B. Batlogg, *Appl. Phys. Lett.*, 2000, **77**, 3776–3778.
- 96 C. W. Struijk, A. B. Sieval, J. E. J. Dakhorst, M. van Dijk, P. Kimkes, R. B. M. Koehorst, H. Donker, T. J. Schaafsma, S. J. Picken, A. M. van de Craats, J. M. Warman, H. Zuilhof and E. J. R. Sudhölter, *J. Am. Chem. Soc.*, 2000, **122**, 11057–11066.
- 97 J. Li, F. Dierschke, J. Wu, A. C. Grimsdale and K. Müllen, *J. Mater. Chem.*, 2006, **16**, 96–100.
- 98 Z. Chen, A. Lohr, C. R. Saha-Möller and F. Würthner, *Chem. Soc. Rev.*, 2009, **38**, 564–584.
- 99 T. Ye, R. Singh, H.-J. Butt, G. Floudas and P. E. Keivanidis, *ACS Appl. Mater. Interfaces*, 2013, **5**, 11844–11857.
- 100 A. Sharenko, C. M. Proctor, T. S. van der Poll, Z. B. Henson, T.-Q. Nguyen and G. C. Bazan, *Adv. Mater.*, 2013, **25**, 4403–4406.
- 101 X. Guo, N. Zhou, S. J. Lou, J. Smith, D. B. Tice, J. W. Hennek, R. P. Ortiz, J. T. L. Navarrete, S. Li, J. Strzalka, L. X. Chen, R. P. H. Chang, A. Facchetti and T. J. Marks, *Nat. Photonics*, 2013, **7**, 825–833.
- 102 W. Jiang, L. Ye, X. Li, C. Xiao, F. Tan, W. Zhao, J. Hou and Z. Wang, *Chem. Commun.*, 2013, **50**, 1024–1026.
- 103 D. J. Burke and D. J. Lipomi, *Energy Environ. Sci.*, 2013, **6**, 2053–2066.
- 104 T. P. Osedach, T. L. Andrew and V. Bulović, *Energy Environ. Sci.*, 2013, **6**, 711–718.

- 105 Y. Zhong, B. Kumar, S. Oh, M. T. Trinh, Y. Wu, K. Elbert, P. Li, X. Zhu, S. Xiao, F. Ng, M. L. Steigerwald and C. Nuckolls, *J. Am. Chem. Soc.*, 2014, **136**, 8122–8130.
- 106 Q. Yan, Y. Zhou, Y.-Q. Zheng, J. Pei and D. Zhao, *Chem. Sci.*, 2013, **4**, 4389–4394.
- 107 S. Subramaniyan, H. Xin, F. S. Kim, S. Shoaee, J. R. Durrant and S. A. Jenekhe, *Adv. Energy Mater.*, 2011, **1**, 854–860.
- 108 J. T. Bloking, X. Han, A. T. Higgs, J. P. Kastrop, L. Pandey, J. E. Norton, C. Risko, C. E. Chen, J.-L. Brédas, M. D. McGehee and A. Sellinger, *Chem. Mater.*, 2011, **23**, 5484–5490.
- 109 X. Guo, F. S. Kim, S. A. Jenekhe and M. D. Watson, *J. Am. Chem. Soc.*, 2009, **131**, 7206–7207.
- 110 A. D. Hendsbee, C. M. Macaulay and G. C. Welch, *Dyes Pigments*, 2014, **102**, 204–209.
- 111 A. D. Hendsbee, J.-P. Sun, L. R. Rutledge, I. G. Hill and G. C. Welch, *J. Mater. Chem. A*, 2014, **2**, 4198–4207.
- 112 J. D. Douglas, M. S. Chen, J. R. Niskala, O. P. Lee, A. T. Yiu, E. P. Young and J. M. J. Fréchet, *Adv. Mater.*, 2014, **26**, 4313–4319.
- 113 A. F. Eftaiha, J.-P. Sun, A. D. Hendsbee, C. Macaulay, I. G. Hill and G. C. Welch, *Can. J. Chem.*, 2014, **92**, 932–939.
- 114 O. K. Kwon, J.-H. Park, S. K. Park and S. Y. Park, *Adv. Energy Mater.*, 2015, **5**, 1400929(1)–1400929(6).
- 115 B.-K. An, J. Gierschner and S. Y. Park, *Acc. Chem. Res.*, 2012, **45**, 544–554.
- 116 S. W. Yun, J. H. Kim, S. Shin, H. Yang, B.-K. An, L. Yang and S. Y. Park, *Adv. Mater.*, 2012, **24**, 911–915.
- 117 K. N. Winzenberg, P. Kemppinen, F. H. Scholes, G. E. Collis, Y. Shu, T. B. Singh, A. Bilic, C. M. Forsyth and S. E. Watkins, *Chem. Commun.*, 2013, **49**, 6307–6309.
- 118 D. Chandran and K.-S. Lee, *Macromol. Res.*, 2013, **21**, 272–283.
- 119 P. Sonar, G.-M. Ng, T. T. Lin, A. Dodabalapur and Z.-K. Chen, *J. Mater. Chem.*, 2010, **20**, 3626–3636.
- 120 X. Guo, M. Zhang, J. Tan, S. Zhang, L. Huo, W. Hu, Y. Li and J. Hou, *Adv. Mater.*, 2012, **24**, 6536–6541.
- 121 Y. Zhang, J. Zou, H.-L. Yip, K.-S. Chen, D. F. Zeigler, Y. Sun and A. K.-Y. Jen, *Chem. Mater.*, 2011, **23**, 2289–2291.
- 122 W. Zhang, J. Smith, S. E. Watkins, R. Gysel, M. McGehee, A. Salleo, J. Kirkpatrick, S. Ashraf, T. Anthopoulos, M. Heeney and I. McCulloch, *J. Am. Chem. Soc.*, 2010, **132**, 11437–11439.